NASA TECHNICAL MEMORANDUM

NASA TM-78928

NASA TM-78928

END-WALL BOUNDARY LAYER PREDICTION FOR AXIAL COMPRESSORS

by Peter M. Sockol
Lewis Research Center
Cleveland, Ohio

TECHNICAL PAPER to be presented at the
Eleventh Fluid and Plasma Dynamics Conference
sponsored by the American Institute of Aeronautics
and Astronautics
Seattle, Washington, July 10-12, 1978

END-WALL BOUNDARY LAYER PREDICTION FOR AXIAL COMPRESSORS

by Peter M. Sockol*

National Aeronautics and Space Administration
Lewis Research Center
Cleveland, Ohio 44135

ABSTRACT

An integral boundary layer procedure has been developed for the computation of viscous and secondary flows along the annulus walls of an axial compressor. The procedure is an outgrowth and extension of the pitch-averaged methods of Mellor and Horlock. In the present work secondary flow theory is used to develop approximations for the velocity profiles inside a rotating blade row and for the blade force deficit terms in the momentum integral equations. The computer code based on this procedure has been iteratively coupled to a quasi-one-dimensional model for the external inviscid flow. Computed results are compared with measurements in a compressor cascade.

E-9668

NOMENCLATURE

A,B	profile parameters, eq. (9)
b	angular blade spacing, fig. 2
C_a	axial projection of blade chord
C_E	entrainment coefficient, eq. (19)
C_{fs},C_{ft}	skin friction coefficients, eq. (18)
D_t,D_x	force deficits, eqs. (16) and (17)
$f(y_t)$	law of wall function, eq. (25)
F_t,f_t	external and local values of blade force
n	power-law exponent, eq. (10)
P,p	external and local static pressure
q_s,q_t	components of friction velocity
$\vec{r}$	radius vector from axis

*Research Engineer, Computational Fluid Mechanics Branch.

s,t,y	intrinsic coordinates, fig. 2
U_s, U_t	components of wheel speed $\vec{\Omega} \times \vec{r}$
$\vec{u}$	rotational velocity field, $\vec{W} - \vec{w}$
$\vec{V}, \vec{v}$	external and local absolute velocities
$\vec{W}, \vec{w}$	external and local relative velocities
W	magnitude $\lvert\vec{W}\rvert$ of velocity $\vec{W}$
x,θ,y	cylindrical coordinates, fig. 1
α	arc tangent of end-wall slope, fig. 1
β	external flow angle, fig. 2
Δp	pressure difference across pitch, $p_2 - p_1$
δ	shear layer thickness
δ^*_α	displacement thickness, eq. (14)
ζ	power-law function, eq. (10)
η_α	y integral of vorticity component
η^*_α	integral of η_α, eq. (7)
$\theta_{\alpha\beta}$	momentum thickness, eq. (14)
κ_s, κ_t	intrinsic curvatures, eq. (15)
κ_x, κ_y	cylindrical curvatures
λ	reciprocal length, $\pi/\phi b \cos\beta)$
μ_α	vorticity parameter, eq. (35)
ν_α	thickness integral, eq. (23)
ρ	density
τ	scaled θ coordinate
$\tau_{0\alpha}$	wall shear-stress component
ϕ	velocity potential of external flow, eq. (1)
$\vec{\psi}$	vector potential for velocity $\vec{u}$, eq. (1)

$\vec{\Omega}$ angular rotation vector

$\vec{\omega}$ absolute vorticity

Subscripts:

0 denotes value at end wall, y = 0

1,2 denotes value at blade surface

Superscripts:

$\bar{}$ denotes pitch-average

$^{+}$ Denotes average of blade surface values

1. INTRODUCTION

The three-dimensional viscous flows along the annulus walls of an axial compressor are known to play a major role in the performance of the machine. The turning of the shear layers by the blades and the relative motion between the end wall and the unshrouded blade tips produce secondary flows most of whose energy is ultimately lost. The displacement effects of the viscous layers can produce substantial local modifications in the pressure field of the external inviscid flow. The prediction of the significant features of these flows is the goal of the present work.

Most of the existing analyses of end-wall flows have followed one of two approaches. The first employs secondary flow theory in the small-shear large-disturbance approximation. An upstream primary vorticity is convected and distorted by a turning irrotational flow. The resulting streamwise vorticity component induces secondary velocities which are calculated by a stream function solution in a cross-sectional plane. Work in this area has been reviewed by Horlock and Lakshminarayana (ref. 1) and more recently by Horlock (ref. 2). This technique can give quite acceptable values for the distribution of flow angle downstream of a blade row, but it cannot predict the blockage and loss associated with the end-wall flow.

The second approach, developed by Mellor and Wood (ref. 3) and Horlock and Perkins (ref. 4), employs integral boundary layer techniques. The three-dimensional equations of motion are averaged across the blade pitch and then integrated across the shear layer normal to the end wall. While the usual boundary-layer approximation is applied to the shear stress, the pressure variation normal to the end wall is not neglected since the blade spacing may be comparable to the shear layer thickness. In principle these equations can predict both the blockage and loss in

the end-wall region; however, in common with all integral procedures, many approximations are required to evaluate important terms in the equations. One promising approach, which has been investigated by Horlock (refs. 4 and 5), is to use secondary flow theory to model some of the terms arising from three-dimensional effects. To date the integral procedures have supplied useful predictions of the overall effects of end-wall flow on blade-row performance. They have not, however, provided the information on conditions within a blade passage needed in our expanded efforts to calculate the flow through a compressor stage.

In the present work secondary flow theory is employed in a number of ways to improve the integral boundary layer technique. First the velocity profiles inside a rotating or stationary blade passage are expressed in terms of integrals of the pitch-averaged absolute vorticity components, which are in turn approximated by simple parametized forms. The velocity profiles are used not only to evaluate the various integral thicknesses, but also to calculate the effects of the pressure gradient normal to the end wall. Finally, the small-shear large-disturbance approximation is used to obtain the streamwise vorticity near the outer edge of the shear layer. Additional auxiliary information is provided by three-dimensional extensions to the law of the wall and to Head's entrainment equation (ref. 6).

The solution of the resulting ordinary differential equations for a multi-stage axial compressor has been developed into a computer code. Initial calculations with this code were performed for the case of the compressor cascade of Papailiou, Flot, and Matheu (ref. 7). The external flow was obtained from an inviscid calculation (ref. 8) in which the blockage was distributed approximately in accord with the measured values. The resulting end-wall predictions were extremely sensitive to the assumed blockage variation inside the blade passage; an interactive calculation was apparently necessary. For simplicity in checking out the end-wall code a quasi-one-dimensional model was devised to represent the external inviscid flow (ref. 9). The axial velocity depends on the combined end-wall and blade blockage and the tangential velocity varies at a rate determined primarily by the turning of the blade mean camber line. When this model is allowed to interact iteratively with the end-wall calculation, a satisfactory prediction scheme results. Comparisons between theory and experiment are presented for the data of reference 7.

2. BASIC ASSUMPTIONS

The fluid equations are written for a reference frame fixed with respect to a rotating blade row. The two coordinate systems used in this frame are shown in figures 1 and 2. One is a cylindrical system with x along a surface meridion, θ circumferential, and y normal to the end-wall. The second is an intrinsic system with s and t, respectively, along and transverse to the streamlines of the external inviscid flow. The variations of the external velocity $\vec{W}$ with y and flow angle β with θ and y are neglected.

In the evaluation of the secondary flow, and subsequently, the blade force deficit, the blade spacing rb is taken to be of the same order as the shear layer thickness δ. Hence, we assume that velocity gradients in the y and t directions are both large compared to those in the s direction with the possible exception of a small region near the blade leading edge. Both δ and rb are assumed small compared to the blade height.

In the vicinity of the blades we neglect the blade boundary layers and assume slip flow along each surface. Downstream of a blade row we neglect the viscous wakes and assume the secondary flow to be confined by vortex sheets which follow the external flow streamlines from the trailing edge. At the leading edge of a following blade row the pitch-averaged vorticity and velocity components are taken to be continuous. Although relative motion is permitted between the blades and the end-wall, no allowance is made for finite tip-clearance flows.

Finally, we note that compressibility is included by allowing the external density ρ to vary with x. The variations of ρ with y and θ are neglected.

3. VELOCITY PROFILES AND SECONDARY FLOW

In this section an approximate solution for secondary flow is used to develop expressions for the velocity profiles. The analysis is an extension of a similar one by Horlock (ref. 5). A more detailed presentation is given in reference 9.

The velocity $\vec{w}$ relative to the blades is split into two parts, $\vec{w} = \vec{W} - \vec{u}$, with $\vec{W}$ and $\vec{u}$ expressed as

$$\vec{W} = \nabla\phi - \vec{\Omega} \times \vec{r}, \qquad \vec{u} = \nabla \times \vec{\psi} \tag{1}$$

and $\vec{u} \to 0$ for $y >> \delta$ with $\nabla \cdot \vec{\psi} = 0$. The absolute vorticity $\vec{\omega}$ and the vector potential $\vec{\psi}$ are related by

$$\nabla^2\vec{\psi} \approx \vec{\omega} \tag{2}$$

We neglect Bernouli surface rotation and set $\omega_y \approx \psi_y \approx 0$. Then the components of $\vec{u}$ can be written

$$u_s \approx -\frac{\partial\psi_t}{\partial y}, \qquad u_t \approx \frac{\partial\psi_s}{\partial y}, \qquad u_y \approx \frac{\partial\psi_\theta}{\partial x} - \frac{2}{rb}\sec\beta\,\frac{\partial\psi_s}{\partial\tau} \tag{3}$$

where $\tau = 2(\theta - \theta_m)/b$ and the partial $\partial/\partial x$ is taken at constant τ. Now $\partial/\partial x = \cos\beta\ \partial/\partial s$ and we assume $\partial/\partial s \approx 0$, hence equation (2) is approximated by

$$\left(\frac{\partial^2}{\partial y^2} + \frac{4}{\pi^2}\lambda^2 \frac{\partial^2}{\partial \tau^2}\right)\vec{\psi} = \vec{\omega} \tag{4}$$

with $\lambda = \pi/(rb \cos \beta)$. The approximate solution for ψ_s is

$$\psi_s \approx \frac{\pi}{2} \bar{\psi}_s(y) \cos \frac{\pi}{2} \tau \tag{5}$$

$$\bar{\psi}_s \approx \eta_s^* \delta e^{-\lambda y} - \int_y^\delta \eta_s(y_1) dy_1 \tag{6}$$

$$\eta_s^* = \frac{1}{\delta} \int_0^\delta \eta_s(y) dy \tag{7}$$

where $\bar{\psi}_\alpha$ is the average of ψ_α across the pitch and $\partial \eta_\alpha / \partial y \equiv \bar{\omega}_\alpha$ with $\eta_\alpha = 0$ for $y > \delta$. The primary component ψ_t is simply approximated by its average value

$$\psi_t \approx \int_0^y \eta_t(y_1) dy_1 \tag{8}$$

Equations (2) and (5) to (8) can be combined to give velocity profiles once approximations for the vorticity components are established.

Absolute Vorticity

Consider first an axisymmetric boundary layer on a stationary end-wall upstream of a rotor. For this case $\lambda = 0$. The components $\eta_{t'}$ and $\eta_{s'}$ in the absolute frame are approximated by

$$\left.\begin{aligned} \eta_{t'} &= -(\bar{V} - \bar{v}_{s'}) \approx -\bar{V}(1 - \zeta) \\ \eta_{s'} &= -\bar{v}_{t'} \approx -\bar{V}(1 - \zeta)\zeta[A(1 - \zeta) + B\zeta] \end{aligned}\right\} \tag{9}$$

with

$$\zeta = \begin{cases} (y/\delta)^{1/n}, & y \le \delta \\ 1, & y > \delta \end{cases} \tag{10}$$

The parameters δ, n, A, and B will be permitted to vary with x. The streamwise component $\overline{v}_s$, has been given a simple power-law profile and the cross-flow $\overline{v}_t$, approximates Johnston's triangular form (ref. 10) whenever A and B have the same sign.

The components η_t and η_s in the relative frame are given by

$$\left.\begin{aligned} \eta_t &\approx -(\overline{W} + U_s)(1 - \zeta) - U_t(1 - \zeta)\zeta[A(1 - \zeta) + B\zeta] \\ \eta_s &\approx -(\overline{W} + U_s)(1 - \zeta)\zeta[A(1 - \zeta) + B\zeta] + U_t(1 - \zeta) \end{aligned}\right\} \tag{11}$$

where U_α are components of the wheel speed $\vec{\Omega} \times \vec{r}$. Inside the rotor $\lambda > 0$ and W varies with τ as well as x. We retain equations (11) but recognize that the velocity profiles obtained from them will not in general satisfy no slip at the wall. This is especially true at a rotating rotor hub. The no slip condition is met by introducing a very thin region adjacent to $y = 0$ in which the velocity profiles are matched to a three-dimensional law of the wall. The mechanics of this are taken up in the section on wall shear stress.

Leading-Edge Region

Whenever there is significant cross-flow relative to the blades upstream of the leading edge, the assumption $\partial/\partial s \approx 0$ is invalid. The cross-flow must be turned by the blade, and it is only after some distance inside the blade row that the passage vortex represented by equation (6) is formed. This situation can be modeled by the addition of a term in x and y to $\overline{\psi}_s$ in equation (6). For the case of a rotor tip, as described in the preceding section, this term has the value $\eta_s^* \delta[1 - \exp(-\lambda y)]$ at the leading edge and it can be represented as a Fourier integral inside the blade row (ref. 9). The displacement effect arising from this term can be shown to decay exponentially with distance x from the leading edge. This might be used to obtain a suitable approximation to the Fourier integral. This possibility is being investigated.

4. VISCOUS EQUATIONS

The momentum integral equations in the intrinsic system together with the entrainment equation are written in a form similar to that of Hirsch (ref. 11). A complete derivation is given in reference 9. In this section the preceding velocity profiles are used to develop approximations to the blade force deficit, wall shear stress, and entrainment rate.

The momentum integral equations are

$$\frac{d\overline{\theta}_{sx}}{dx} + \overline{\theta}_{sx}\frac{d}{dx}\ln(rb\rho\overline{W}^2) + \frac{1}{\overline{W}}\left(\overline{\delta_s^*\frac{\partial W}{\partial s}} + \overline{\delta_t^*\frac{\partial W}{\partial t}}\right)$$

$$- \kappa_t\overline{\theta}_{ts} + \kappa_s\overline{\theta}_{tt} + 2\kappa_x\tilde{U}\overline{\delta_t^*} \approx D_x\cos\beta + \frac{1}{2}C_{fs} \qquad (12)$$

$$\frac{d\overline{\theta}_{tx}}{x} + \overline{\theta}_{tx}\frac{d}{dx}\ln(rb\rho\overline{W}^2) - \kappa_s\overline{\theta}_{ts} + \kappa_t\left(\overline{\theta}_{ss} + \frac{1}{\overline{W}}\overline{W\delta_s^*}\right)$$

$$- 2\kappa_x\tilde{U}\overline{\delta_s^*} \approx -D_x\sin\quad + D_t + \frac{1}{2}C_{ft} \qquad (13)$$

where

$$\left.\begin{aligned}\overline{W}_s\delta_\alpha^* &= \int_0^\infty (W_\alpha - w_\alpha)dy = \int_0^\infty u_\alpha\,dy \\ \overline{W}^2\theta_{\alpha\beta} &= \int_0^\infty (W_\alpha - w_\alpha)w_\beta\,dy = \overline{W\delta_\alpha^*}\overline{W}_\beta - \int_0^\infty u_\alpha u_\beta\,dy\end{aligned}\right\} \qquad (14)$$

$$\kappa_s = -\frac{\partial\beta}{\partial t} + \kappa_x\cos\beta, \qquad \kappa_t = \frac{\partial\beta}{\partial s} - \kappa_x\sin\beta \qquad (15)$$

$$D_x = -(\rho\overline{W}^2)^{-1}\frac{d}{dx}\int_0^\infty (\overline{P} - \overline{p})dy = -(\rho\overline{W}^2)^{-1}\frac{d}{dx}\int_0^\infty \frac{\partial\overline{P}}{\partial y}\,y\,dy \qquad (16)$$

$$D_t = (\rho\overline{W}^2)^{-1}\int_0^\infty (F_t - f_t)dy = (\rho\overline{W}^2)^{-1}\int_0^\infty \frac{\partial f_t}{\partial y}\,y\,dy \qquad (17)$$

$$C_{f\alpha} = 2(\rho\overline{W}^2)^{-1}\,\overline{\tau}_{0\alpha} \qquad (18)$$

with $\kappa_x = -\partial r/r\,\partial x$, $\tilde{U} = U/\overline{W}$, and $f_t = -\Delta P/(rb\cos\beta)$. Here $\Delta P = P_2 - P_1$ is the pressure difference across the pitch. The upper limit on y is taken very large because the secondary flow extends well beyond the edge of the shear layer, $y = \delta$.

The entrainment equation is written

$$\frac{d}{dx}\left(\delta\cos\beta - \overline{\delta_x^*} + \overline{\delta_x^\infty}\right) + \left(\delta\cos\beta - \overline{\delta_x^*} + \overline{\delta_x^\infty}\right)\frac{d}{dx}\ln(rb\rho\overline{W}) = C_E \quad (19)$$

where $C_E\overline{W}$ is the entrainment rate at $y = \delta$ and

$$\overline{W}\delta_\alpha^\infty = \int_\delta^\infty (\overline{w}_\alpha - w_\alpha)dy = \int_\delta^\infty u_\alpha\, dy \quad (20)$$

The integral thicknesses are evaluated from the profiles of equations (3), (6), (8), and (11) in reference 9. The averages in equations (12) and (13) are approximated by setting $\overline{w_\alpha w_\beta} \approx \overline{w}_\alpha \overline{w}_\beta$. Estimates of the neglected terms indicate that they contribute less than ten percent even for highly loaded blades.

Force Deficits

Let $\partial/\partial s$ be of order one, O(1), and assume that rb is $O(\delta)$, then from the y momentum equation

$$(\rho\overline{W}^2)^{-1}\frac{\partial\overline{P}}{\partial y} = O(1), \qquad (\rho\overline{W}^2)^{-1}\frac{\partial f_t}{\partial y} = O\left(\frac{1}{\delta}\right)$$

When these relations are substituted into equations (16) and (17), it is seen that D_x is $O(\delta^2)$ and D_t is $O(\delta)$. Since equations (12) and (13) are only correct to $O(\delta)$ we neglect D_x. An equation for f_t is obtained by evaluating the y momentum equation at the blade surfaces where $w_t = 0$.

$$\frac{1}{\rho}\frac{\partial f_t}{\partial y} \approx \frac{w_s^+}{rb}\frac{\partial}{\partial x}(\Delta w_y) + \frac{\Delta w_s}{rb}\frac{\partial w_y^+}{\partial x} + \frac{1}{rb}\frac{\partial}{\partial y}(w_y^+\,\Delta w_y)\sec\beta$$

$$+ 2\kappa_y(w_\theta^+ + U)\frac{\Delta w_\theta}{rb}\tan\beta + \text{viscous terms} \quad (21)$$

where $w_\alpha^+ = \frac{1}{2}(w_{\alpha 1} + w_{\alpha 2})$ and $\kappa_y = -\partial r/r\,\partial y$. The integrand in equation (17) is only significant for y of $O(\delta)$ or larger where $w_\theta^+ \approx W^+ \approx \overline{W}$ and the viscous terms in equation (21) are small. Also from equations (3) and (5), away from the leading edge, $w_y^+ \approx 0$. The first term on the right of equation (21) must be retained, however, since $\Delta w_y = w_{y2} - w_{y1}$ is $O(\overline{w}_t)$. With these approximations, substitution of equation (21) into equation (17) gives

$$D_t \approx -\cos\beta \frac{d\nu_y}{dx} - \nu_y \cos\beta \frac{d}{dx} \ln(rb\overline{W}\cos\beta) - 2\kappa_y(\sin\beta + \tilde{U})\nu_s \sin\beta \tag{22}$$

with

$$\overline{W}\nu_\alpha = (rb\cos\beta)^{-1} \int_0^\infty \Delta(W_\alpha - w_\alpha)y\, dy = \frac{\lambda}{\pi} \int_0^\infty \Delta u_\alpha y\, dy \tag{23}$$

The thicknesses ν_α are evaluated in reference 9.

Wall Shear Stress

We assume the flow in a thin region adjacent to $y = 0$ is collateral and obeys a three-dimensional law of the wall,

$$\overline{w}_s - w_{s0} = q_s f(y_+), \qquad \overline{w}_t - w_{t0} = q_t f(y_+) \tag{24}$$

where

$$f(y_+) = \frac{1}{0.41} \ln y_+ + 5, \qquad y_+ = yq/\nu \tag{25}$$

and $\overline{w}_{\alpha 0}$ are the components of the end-wall velocity relative to the blades. The skin friction coefficients are related to the friction velocities q_α by $C_{f\alpha} = 2qq_\alpha/\overline{W}^2$. At $y \to 0$, equations (3), (6), (8), and (11) give

$$\left.\begin{aligned} \overline{w}_s - w_{s0} &= -(U_s + w_{s0}) + [(\overline{W} + U_s) - U_t A]\zeta \\ \overline{w}_t - w_{t0} &= -(U_t + w_{t0}) + (\lambda\delta)\eta_s^* + [(\overline{W} + U_s)A + U_t]\zeta \end{aligned}\right\} \tag{26}$$

Matching equations (24) and (26) at $y/\delta = \hat{y}$ gives

$$\left.\begin{aligned} q_s f(\hat{y}_+) &= -(U_s + w_{s0}) + [(\overline{W} + U_s) - U_t A]\hat{y}^{1/n} \\ q_t f(\hat{y}_+) &= -(U_t + w_{t0}) + (\lambda\delta)\eta_s^* + [(\overline{W} + U_s)A + U_t]\hat{y}^{1/n} \end{aligned}\right\} \tag{27}$$

with $\hat{y}_+ = \hat{y}\delta q/\nu$. Equations (27) can be solved iteratively for q_s and q_t. This formulation enables the flow to respond to sudden changes in the end-wall velocity such as those which occur at a rotor hub. Note that $\hat{y} = 0.1$ gives a good value for C_f in a two-dimensional boundary layer.

Entrainment Rate

In two-dimensional flows the entrainment rate $C_E\overline{W}$ is given by (ref. 12)

$$C_E\overline{W} \approx -\frac{1}{\rho}\left(\frac{\partial \tau_{ys}/\partial y}{\partial w_0/\partial y}\right)_{y=\delta} \approx -\left(\frac{\partial \nu_T}{\partial y}\right)_{y=\delta} \tag{28}$$

where ν_T is the eddy viscosity. Since C_E is a scalar, we assume with Bradshaw (ref. 13) that the same relation holds in three-dimensional flow. If we approximate ν_T by

$$\nu_T \approx \ell_M^2\left(\omega_s^2 + \omega_t^2\right)^{1/2} \tag{29}$$

where ℓ_M is the mixing length, then equations (11) and (29) as $y \to \delta$ give

$$\nu_T \approx (\nu_T)_{2D}\tilde{V}(1 + B^2)^{1/2}, \qquad (\nu_T)_{2D} \approx \ell_M^2\frac{\overline{W}}{ny} \tag{30}$$

with $\tilde{V} = \overline{V}/\overline{W}$. The expression for $(\nu_T)_{2D}$ is not accurate enough to be used in equation (28). Hence, its derivative is replaced by Head's empirical relation (ref. 6). Thus, we approximate C_E by

$$C_E \approx 0.0306(H^* - 3)^{-0.653}\tilde{V}(1 + B^2)^{1/2} \tag{31}$$

with

$$H^* = 1.535(H - 0.7)^{-2.715} + 3.3 \tag{32}$$

$$H = 1 + 2/n \tag{33}$$

Equation (33) for the streamwise shape factor H follows from the power-law relation equation (10).

5. VORTICITY TRANSPORT

In the outer part of the shear layer, near $y = \delta$, we assume that streamwise vorticity ω_s is convected by the external flow with only the primary component ω_t directly affected by viscous diffusion. This model is similar to that of Louis (ref. 14). In addition pressure and density are taken to be the same as in the external flow where $P \approx P(\rho)$. For these conditions the transport equation for ω_s is (ref. 9)

$$\rho W\frac{\partial}{\partial s}\left(\frac{\omega_s}{\rho}\right) \approx \omega_s\frac{\partial W}{\partial s} + 2\omega_t(\kappa_t W - \kappa_x U) \tag{34}$$

Equation (34) is evaluated with average values for ω_α and W. From equations (11), as $y \to \delta$ and $\zeta \to 1$,

$$\overline{\omega}_\alpha \approx \mu_\alpha \overline{W}/ny \tag{35}$$

$$\mu_t = (1 + \tilde{U}_s) + \tilde{U}_t B, \qquad \mu_s = (1 + \tilde{U}_s)B - \tilde{U}_t \tag{36}$$

with $\tilde{U}_\alpha = U_\alpha/\overline{W}$. Note that y must be much less than δ before ζ departs significantly from one. Finally, equations (34) to (36) are combined to give

$$n \frac{d}{dx}\left(\frac{\mu_s}{n}\right) \approx \mu_s \frac{1}{\rho}\frac{d\rho}{dx} + 2 \sec\beta\, \mu_t(\kappa_t - \kappa_x \tilde{U}) \tag{37}$$

6. INTEGRATION OF THE GOVERNING EQUATIONS

The integral and vorticity equations are written in a combined implicit form

$$\frac{d}{dx} F_i = G_i, \qquad i = 1 \text{ to } 4 \tag{38}$$

The overbars are dropped and all quantities are understood to take their average values. From equations (12), (13), (19), (22), and (37) we write

$$\left.\begin{aligned} F_1 &= \delta \cos\beta - \delta_x^* + \delta_x^\infty, \qquad F_2 = \theta_{sx} \\ F_3 &= \theta_{tx} + v_y \cos\beta, \qquad F_4 = \mu_s/n \end{aligned}\right\} \tag{39}$$

$$
\left.
\begin{aligned}
G_1 &= -F_1 \frac{d}{dx} \ln(rb\rho W) + C_E \\
G_2 &= -\theta_{sx} \frac{d}{dx} \ln(rb\rho W^2) - \delta_x^* \frac{1}{W} \frac{dW}{dx} + \kappa_t \theta_{ts} - \kappa_s \theta_{tt} \\
&\qquad - 2\kappa_x \tilde{U} \delta_t^* + \frac{1}{2} C_{fs} \\
G_3 &= -\theta_{tx} \frac{d}{dx} \ln(rb\rho W^2) + \kappa_s \theta_{ts} - \kappa_t(\theta_{ss} + \delta_s^*) + 2\kappa_x \tilde{U} \delta_s^* \\
&\qquad - \nu_y \cos\beta \frac{d}{dx} \ln(rbW) - 2\kappa_y(\sin^2\beta + \tilde{U}_s)\nu_s + \frac{1}{2} C_{ft} \\
G_4 &= \frac{\mu_s}{n} \frac{1}{\rho} \frac{d\rho}{dx} + 2 \sec\beta \frac{\mu_t}{n} (\kappa_t - \kappa_x \tilde{U})
\end{aligned}
\right\} \qquad (40)
$$

Numerical Procedure

Equations (38) are rewritten in an explicit matrix form

$$M(x,Y) \frac{dY}{dx} = G(x,Y) - F_x(x,Y) \qquad (41)$$

or

$$\frac{dY}{dx} = M^{-1}(G - F_x) \equiv D \qquad (42)$$

where Y is the unknown vector (δ, n, A, B), M is the Jacobian matrix $\partial F/\partial Y$, and $F_x = \partial F/\partial x$. The elements of M and F_x are given in reference 9. Equation (42) is integrated by the fourth-order Runge-Kutta method with Gaussian elimination used to find D at each step.

7. DISCUSSION OF RESULTS

The end-wall theory has been used to predict the low speed flow through a linear cascade of compressor blades as reported in reference 7. A detailed set of data for the heavily loaded case B has been obtained from the authors (ref. 15). In this flow a set of NACA 65-(12A10)-10 blades at 30 degrees stagger was used to turn the flow from $\beta = 56.6$ degrees to $\beta = 25.2$ degrees. The data taken upstream of the cascade reveal the presence of a significant cross-flow extending to mid-span. The

shear layer, however, is confined to a thickness of less than one fourth the blade height. Since the theory, in its present form, is incapable of properly treating this situation, the computation was performed with the upstream cross-flow set to zero.

The comparison between theory and experiment is shown in figures 3 to 6. Figures 3 and 4 show the tangent of the flow angle β and the axial velocity V_x against dimensionless distance x/C_a, where C_a is the axial projection of the blade chord, as obtained from the quasi-one-dimensional model of the inviscid flow. The turning rate inside the blade row has been adjusted to produce the agreement in $\tan\beta$ shown in figure 3. However, the figure also shows that the real flow undergoes significant turning before it encounters the leading edge at $x = 0$. The under prediction of V_x in figure 4 indicates that the real flow encounters somewhat greater blockage than predicted in the computation. Figure 5 shows the streamwise displacement and momentum thicknesses, δ_s^*/C_a and θ_{ss}/C_a, against x/C_a. While the close agreement for δ_s^* inside the blade row is probably fortuitous, the general trends for both curves are highly encouraging. There is no point in comparing cross-flow thicknesses, since the upstream cross-flow has been neglected in the computation. Finally, figure 6 shows the blade force deficit D_t against x/C_a. Although there is qualitative agreement, the predicted value is too small by more than a factor of two. The inclusion of a leading edge model which can properly account for the rapid turning of the upstream cross flow should go a long way toward removing this discrepancy.

8. CONCLUSIONS AND RECOMMENDATIONS

In its present form the end-wall prediction scheme has been shown to give at least qualitatively correct results for the pitch-averaged flow through a linear cascade of compressor blades. Naturally many more comparisons with internal flow measurements are needed. However, at least three things must be added before the theory can be used to predict the end-wall flows in an axial compressor:

1. A leading edge model which can treat the rapid turning of an upstream cross-flow and its contribution to the blade force;

2. A model for tip clearance flows and their effect on boundary layer growth;

3. Coupling of the end-wall prediction to a multi-stage though-flow calculation for the inviscid flow.

9. REFERENCES

1. Horlock, J. H. and Lakshminarayana, B., "Secondary Flows: Theory, Experiment, and Application in Turbomachinery Aerodynamics," Annual Review of Fluid Mechanics, Vol. 5, Annual Reviews, Inc., Palo Alto, 1973, pp. 247-280.

2. Horlock, J. H., "Recent Developments in Secondary Flow," AGARD Conference Proceedings no. 214 on Secondary Flows in Turbomachines, pp. 1-1 to 1-18, Mar. 1977.

3. Mellor, G. L. and Wood, G. M., "An Axial Compressor End Wall Boundary Layer Theory," Journal of Basic Engineering, Vol. 93, June 1971, pp. 300-316.

4. Horlock, J. H. and Perkins, H. J., "Annulus Wall Boundary Layers in Turbomachines," AGARD-AG-185, May 1974.

5. Horlock, J. H., "Cross Flows in Bounded Three-Dimensional Turbulent Boundary Layers," Journal of Mechanical Engineering Science, Vol. 15, Aug. 1973, pp. 274-284.

6. Head, M. R., "Cambridge Work on Entrainment," Computation of Turbulent Boundary Layers, Vol. 1, Stanford University, Stanford, Calif., 1969, pp. 188-194.

7. Papailiou, H., Flot, R., and Mathieu, J., "Secondary Flows in Compressor Bladings," Journal of Engineering for Power, Vol. 99, 1977, pp. 211-224.

8. Katsanis, T. and McNally, W. D., "Revised Fortran Program for Calculating Velocities and Streamlines on the Hub-Shroud Midchannel Stream Surface of an Axial-, Radial-, or Mixed-Flow Turbomachine or Annular Duct," NASA TN D-8430, 1977.

9. Sockol, P. M., "End-Wall Boundary Layer Prediction for Axial Compressors," NASA TP to be published.

10. Johnston, J. P., "On the Three-Dimensional Turbulent Boundary Layer Generated by Secondary Flow," Journal of Basic Engineering, Vol. 82, Mar. 1960, pp. 233-248.

11. Hirsch, C., "Flow Prediction in Axial Flow Compressors Including End-Wall Boundary Layers," ASME Paper 76-GT-72, 1976.

12. Head, M. R. and Galbraith, R. A. Mc D., "Eddy Viscosity and Entrainment in Equilibrium Boundary Layers," Aeronautical Quarterly, Vol. 26, Nov. 1975, pp. 229-242.

13. Bradshaw, P., "Calculation of Three-Dimensional Turbulent Boundary Layers," Journal of Fluid Mechanics, Vol. 46, Mar. 1971, pp. 417-445.

14. Louis, J. F., "Rotational Viscous Flow," IX^{e} Congrès International de Mécanique Appliquée, (Proceedings of the 9th International Congress of Applied Mechanics), Vol. 3, Université de Bruxelles, 1957, pp. 306-317.

15. Papailiou, K., Private communication, April 1978.

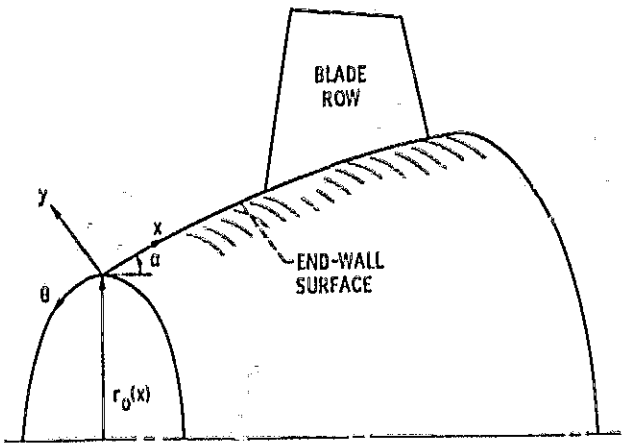

Figure 1. - End-all geometry and cylindrical coordinate system.

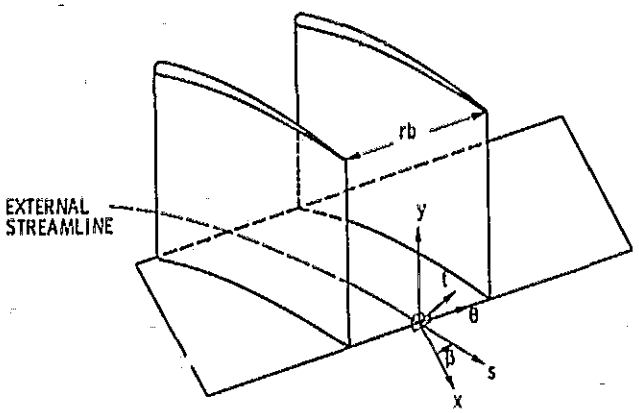

Figure 2. - Cascade geometry and intrinsic coordinate system.

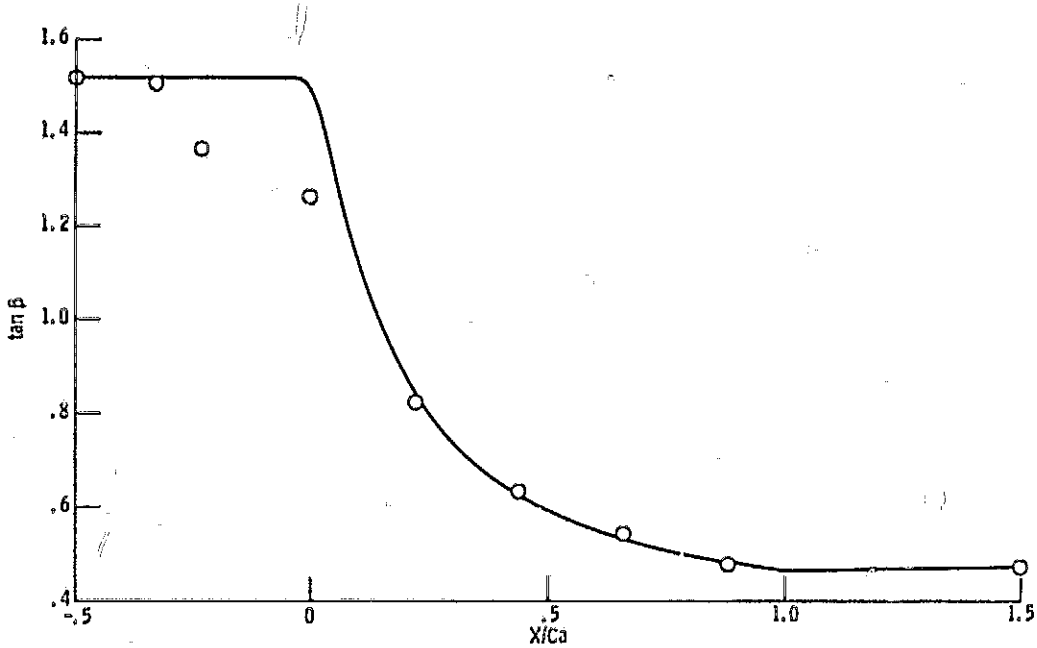

Figure 3. - Tangent of inviscid flow angle vs. distance. theory ——, experiment ○.

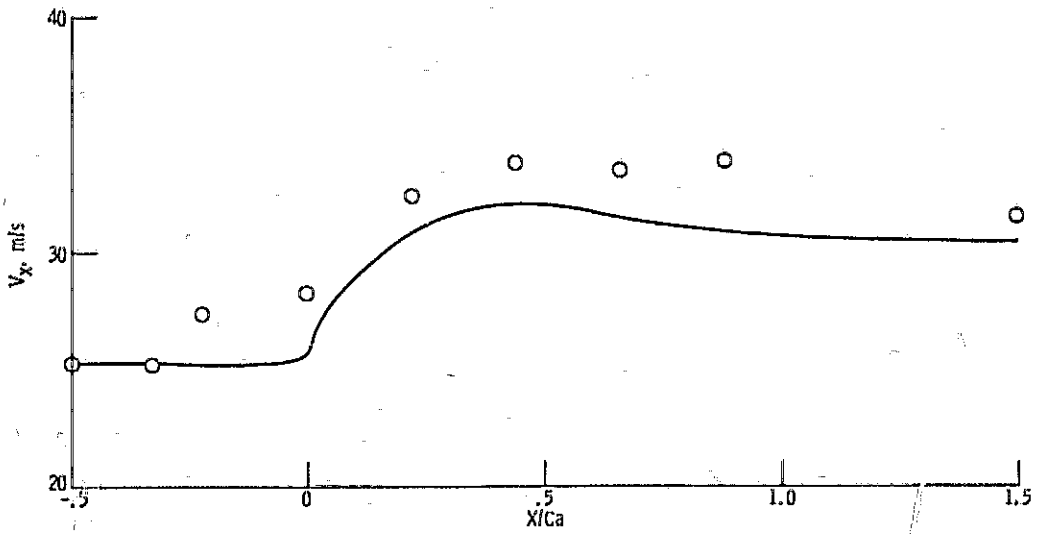

Figure 4. - Inviscid axial velocity vs. distance: theory ——, experiment ○.

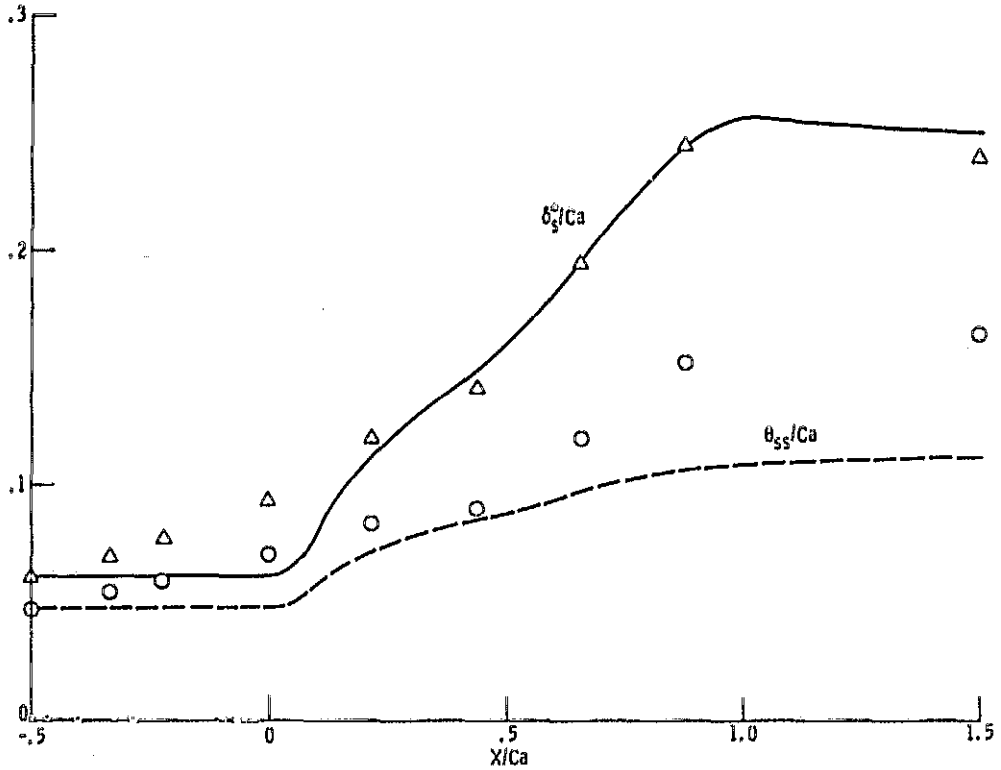

Figure 5. - Streamwise displacement and momentum thickness vs. distance: theory ——, – – – –; experiment △, ○.

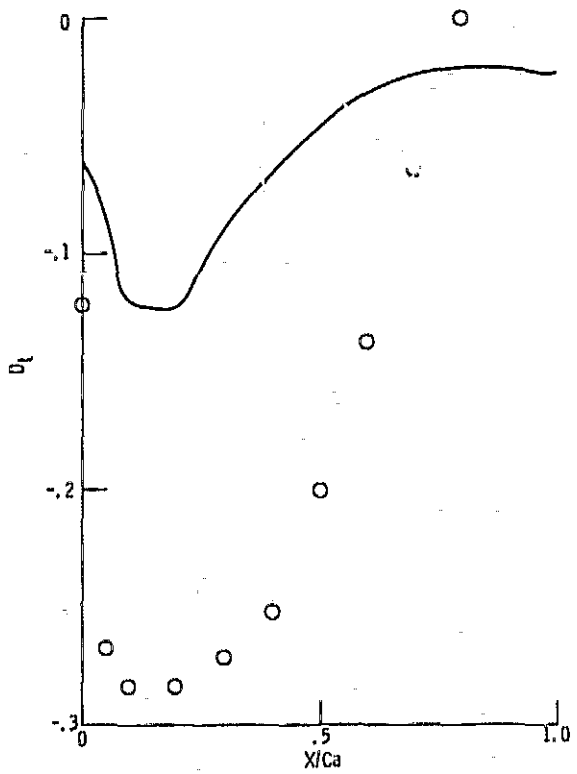

Figure 6. - Blade force deficit vs. distance: theory ——, experiment ○.